A GENERALIZED METHODOLOGY FOR OBTAINING QUANTITATIVE CHARPY DATA FROM TEST SPECIMENS OF NONSTANDARD DIMENSIONS

MICHAEL P. MANAHAN, Sr. *The Pennsylvania State University*
231 Sackett Building, University Park, Pennsylvania 16802

CHRISTOPHER CHARLES *Roy F. Weston, Inc.*
955 L'Enfant Plaza S.W., Washington, D.C. 20024

Received May 15, 1989
Accepted for Publication December 14, 1989

Miniaturized specimen technology enables mechanical behavior determination using a minimum volume of material. A method for obtaining the ductile-brittle transition temperature (DBTT) of ferritic steels was developed using a miniaturized notch test (MNT). Comparisons between conventional and miniaturized specimen DBTTs show that the MNT specimens are capable of delivering a 41-J transition temperature shift with the same accuracy as that obtained using conventional specimens. The work reported here was performed on an American Society for Testing Materials A508 steel. Based on the promising results obtained, future work should be directed toward benchmarking and assessing the uncertainty of the method for other pressure vessel steels.

INTRODUCTION

Miniaturized specimen technology (MST) permits the characterization of mechanical behavior while using a minimum volume of material. Hence, it has many applications, such as nuclear pressure vessel surveillance, failure analysis, and postirradiation testing.[a] It can also be used to characterize the mechanical behavior of in-service structures and components in cases where small pieces of material can be safely cut out. MST has been used in a variety of nuclear applications including fusion materials research,[1] cladding stress-corrosion-cracking studies,[2] fracture behavior of pressure vessels,[3] and steam generator plugging analysis.[4] The intended primary application for the work reported here is pressure vessel surveillance during the life extension period. Miniature specimens have already been included in second-generation boiling water reactor surveillance capsules for the purpose of generating life extension data.[5] The goal of the present study is to examine the feasibility of a fracture mechanics test making use of miniaturized three-point bend (TPB) specimens. A new test, the miniaturized notch test (MNT), was developed to determine the ductile-brittle transition temperature (DBTT) of ferritic steel.

[a]The processes described are explained in part in U.S. patent no. 4,567,774 dated February 4, 1986. A patent application on further improvements of the methodology is pending.

REVIEW OF LITERATURE

A large body of data concerned with size and geometry effects on DBTT determination has been developed over the past 40 yr. An extensive literature review was provided by Charles.[6] Current fracture behavior tests grew out of this large collection of data through American Society for Testing Materials (ASTM) committee work.[7-18]

The early DBTT work was done to identify important test parameters and to arrive at accepted test procedures. Recent work was aimed at miniaturization for postirradiation testing. This work, most notably that of Corwin and Houghland,[19] Lucas et al.,[20] and McConnell et al.,[21] has indicated that Charpy V-notch (CVN) tests, including those for miniaturized specimens, provide only empirical or qualitative data. These authors conclude that the mini-CVN tests are valuable for determining material considerations such as fundamental fracture and flow parameters, the validity of interpolative fracture criteria, valid fracture toughness fibrous crack growth resistance curves, and qualitative data for tracking irradiation behavior and monitoring

relative differences of materials. The ASTM Standard A370-86a suggests that the energy values determined by these tests are "qualitative comparisons . . . [that] cannot be converted into energy figures that would serve for engineering calculations."[7] Further, Lucas et al. state that

> Thus while the behavior of mini-CVN specimens has been found to be qualitatively similar to that of standard CVNs, quantitative comparisons have been found to be only in approximate agreement at best. This is not particularly surprising, since parameters such as transition temperature or ΔTT are functions of an arbitrarily chosen reference energy and are thus sensitive to test conditions and particularly specimen geometry. Thus it would seem that the greater potential for success in using mini-CVNs is to use them to extract more fundamental property information.[20]

While we agree that Charpy testing does not provide fundamental material fracture property data as does the K_{IC} test,[9] for example, we disagree with the conclusions of Lucas et al.[20] and Corwin and Houghland[19] concerning the qualitative aspects of miniature specimen data. Thus, the present study advances and extends the current theory of mini-CVN testing by showing that it is possible to obtain, from miniaturized specimens, quantitative DBTT data that are as accurate as those obtained using conventional ASTM E23 specimens. Work to date by others has focused on one-third or one-fourth size mini-CVN specimens.[19-21] In the present study, the specimen size is chosen close to the continuum limit of the material. For the ASTM A508 steel investigated, this results in a miniaturized specimen volume that is about one-sixteenth the volume of a conventional specimen. This enables as many as eight MNT specimens to be machined from each half of a broken conventional CVN specimen. Further, a new test parameter has been discovered that can be used to relate miniature specimen data with conventional specimen data.

EXPERIMENTAL DESIGN

The experimental design of the miniaturized DBTT test was based on the material microstructure, current testing practice, amount of material available, and desired stress state. These design considerations are discussed in detail in Ref. 22. Material for this work was taken from a special heat of ASTM A508 steel provided by Oak Ridge National Laboratory (ORNL) for crack arrest research as part of the heavy section steel technology program. This steel has been extensively characterized at ORNL as well as Battelle Columbus Laboratories and the University of Maryland. As part of the ORNL program, three different heat treatments were prepared and designated 6, 5A, and 6R in order of increasing toughness and increasing tempering temperature. To confirm the data reported by ORNL (Ref. 23), samples from the three heats were mounted and etched to enhance the ferritic grain structure. Micrographs were made, and the grain size was observed to be between 7.5 and 8.0 (ASTM designation G).

An important limitation in miniaturizing any specimen is the extent of the material's microstructural inhomogeneities. The usual guideline dictates that the specimen be at least five to ten times as large as the characteristic heterogeneity dimension. Microscopy analysis indicated that carbon segregates in slender bands ~0.25 mm wide. Figure 1 is a low-magnification photomicrograph of the steel with heat treatment 6R. The dark regions are believed to be carbon-rich, reflecting an enhanced local density of carbide precipitates. Steel with the lowest tempering temperature (heat treatment 6) exhibited only faint indications of segregation. The reason for this difference is not clear. As a result of these findings, the minimum specimen dimension should be in the range of 3 to 5 mm. For a fracture behavior specimen, this minimum limits the dimensions of the crack plane.

Conventional Charpy specimens were tested both statically and dynamically using the punch and anvil spacing prescribed in Ref. 8. For miniaturized specimens, it was necessary to decrease the punch thickness and anvil spacing. Key experimental parameters used in the first round of experiments are compared in Table I. The phase I work is reported in Ref. 22. As a result of the testing difficulties at higher temperatures, which are described later, the punch and anvil radii had to be decreased to obtain useful data. The key experimental parameters used during the phase II work are also given in Table I. Other procedures and specifications regarding the test temperature, alignment accuracy, and machining tolerances were also in accordance with ASTM E23 specifications.[8]

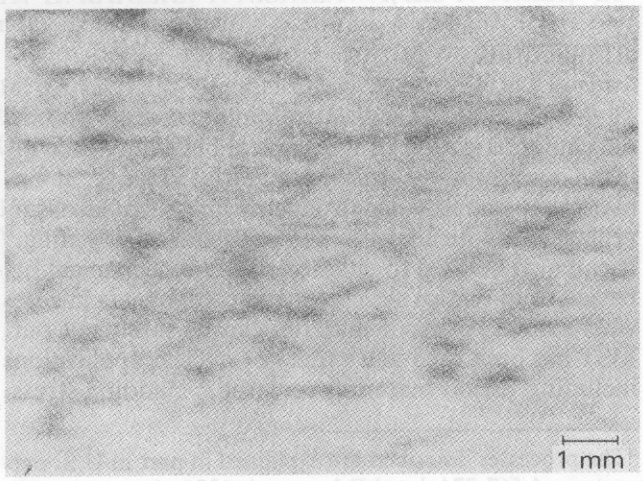

Fig. 1. Low-magnification micrograph of heat treatment 6R showing carbon segregation.

TABLE I

Relevant Anvil Support and Punch Dimensions

	Conventional Charpy Test (ASTM E23) [mm (in.)]	Miniature Specimen Test (Phase I Study) [mm (in.)]	Miniature Specimen Test (Phase II Study) [mm (in.)]
Punch radius	8.00 (0.315)	8.00 (0.315)	0.64 (0.025)
Punch tip width	3.99 (0.157)	2.29 (0.090)	1.27 (0.050)
Anvil radius	1.00 (0.039)	1.00 (0.039)	0.13 (0.005)
Anvil spacing	40.00 (1.575)	11.43 (0.450)	11.68 (0.460)

With regard to material availability, it was assumed that the broken halves of tested Charpy bars would be made available for miniaturization. The miniaturized TPB specimens were sized so that eight specimens could be machined from each half of a conventional broken Charpy specimen. This permits the maximum number of specimens to be produced from a broken Charpy specimen from a nuclear surveillance capsule and still satisfies the material-based size requirements for the steel being investigated.

With regard to the stress state in the vicinity of the notch, the approach adopted for the MNT was to modify the specimen design to increase plastic constraint. Side grooves were machined into the specimen in addition to the notch, as shown in Fig. 2. The important miniaturized specimen design parameters are compared with conventional specimen parameters in Table II.

The effect of the side grooves is illustrated in Fig. 3. The σ_x stress component from the side groove in the thin sample is intended to offset the lack of the through-thickness stress σ_z that is present in the thick specimens. Although the σ_x stress in the miniaturized specimen is not generally uniformly distributed and is not of the same magnitude as the σ_z stress in the thick samples, sufficient constraint can be induced to enable measurement of the DBTT using miniaturized specimens. Historically, side grooving has been used to obtain more uniform crack fronts in fracture toughness testing and to constrain the fracture plane in certain materials. In the present study, the side grooves are brought into close proximity so that their σ_x stress components overlap; the result is a fairly uniform through-thickness stress field.

TABLE II

Comparison of Important Specimen Dimensions

	ASTM Charpy Specimen (mm)	Miniature Specimen (mm)
Thickness, B (crack plane)	10.01	4.83
Depth, H (direction of crack propagation)	10.01	4.83
Length, L	54.99	12.70
Reduced side thickness, B_n	NA[a]	3.86
Notch depth, a	2.01	0.97
Notch-root radius, r	0.25	0.25

[a]NA = not applicable.

DATA ANALYSIS AND RESULTS

Several DBTT criteria are used in different industries. Since nuclear pressure vessel surveillance is the application of current interest, the 41-J (30-ft·lb) energy absorption level was used as a reference. For the three heat treatments, the Charpy DBTTs are as follows: heat treatment 6, 40°C; heat treatment 5A, −7°C; and heat treatment 6R, −29°C. The key element of data interpretation is to be able to find a parameter and an index that relate the miniature and conventional specimens. We have defined the term "parameter" to mean the range variable (e.g., energy, fracture appearance, lateral expansion) and the term "index" to mean the transition temperature indicator (41-J, 0.89-mm lateral expansion). The results of this investigation are discussed below.

Normalized Energy Parameter

The first approach investigated was to normalize the energy parameter and the 41-J index. To allow a heat-to-heat comparison, all the test temperatures for the slow-bend specimens were adjusted by subtracting the appropriate impact-transition temperature. The absorbed energy was divided by the area of the crack plane in an attempt to place the standard Charpy and MNT data on a common basis. Figure 4 shows the conventional Charpy specimen data normalized in this way. The normalizations provide good superposition of the data, as expected. The 41-J (512 kJ/m^2) level occurs at about −45.3°C. This factor accounts for the

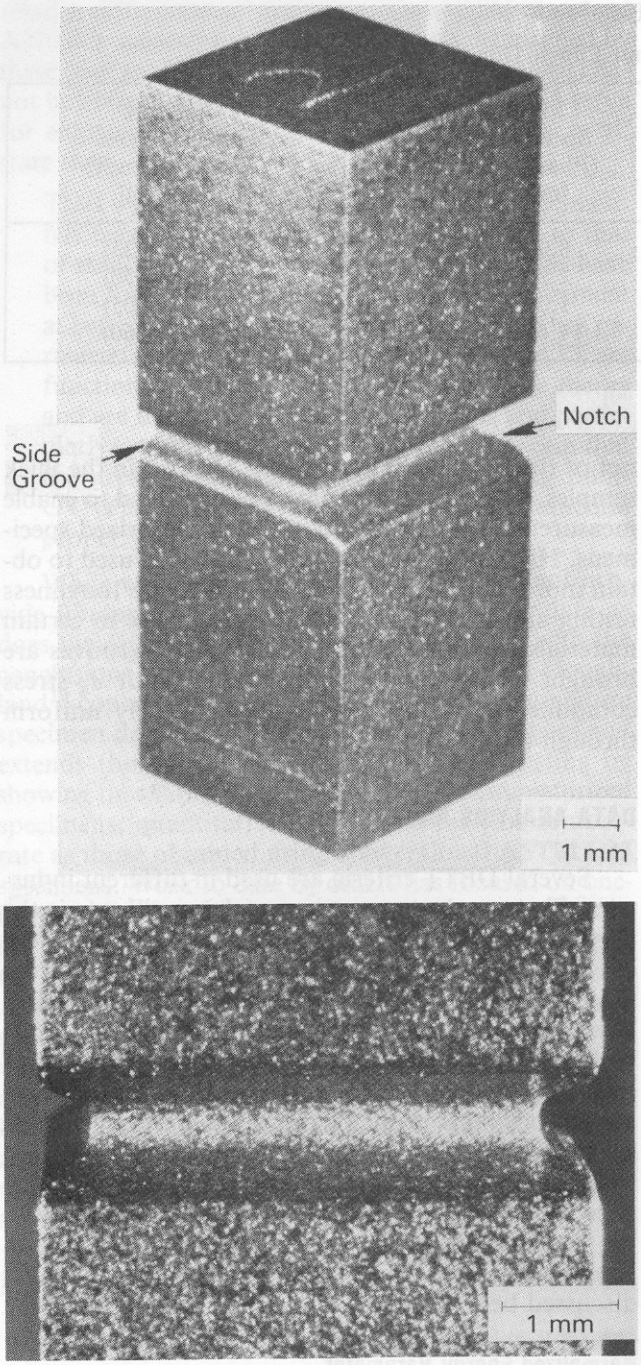

Fig. 2. Miniature specimen showing side grooves and notch.

downward shift in the 41-J index due to static testing. These data were fitted using the statistical analysis methodology reported by Manahan et al.[25,26] Rolfe and Barsom[27] present a correlation for the temperature shift between slow-bend and impact loading. Using this correlation, the expected shift would be ~36°C. This is in reasonable agreement with our data, considering that the correlation is based on the assumption that the onset of the dynamic transition temperature is defined by the intersection of tangent lines drawn from the lower shelf level and the transition region.

Figure 5 shows the results for the phase I MNT study. Two specimens at higher temperatures are off the scale of interest and consequently are not plotted. The superposition is again good at lower temperatures. The use of the miniaturized specimens results in a further downward shift of 76.7°C in temperature, producing a total shift of −122°C between standard impact Charpy tests and slow-bend miniaturized specimen tests.

The miniaturized specimen data in Fig. 5 are scattered at higher temperatures due to experimental difficulties. At higher temperatures, where there is stable crack growth and substantial plastic deformation, the specimens were observed to slip off the flat portion of the anvil and were supported by the curved portion. As a result, it was necessary to scale down the radius of curvature of the anvil and the punch. These changes are essential to measure high transition and upper shelf data. All data gathered during the phase II work were taken using the scaled-down punch and specimen support. The results are presented later.

Tests were run without side grooving the specimens, and the data in the transition region could not be analyzed due to severe plastic deformation. It is essential to use side grooves to increase the transverse stress to the level where there is sufficient constraint to yield transitional behavior over a reasonable temperature range. Thus, the experimental hurdle of DBTT testing near the material continuum limit has been overcome. However, to fully validate the test, the use of the normalized energy parameter and the 512 kJ/m^2 index was investigated to ensure consistency in fracture behavior.

Fracture Appearance

Further work was undertaken during the second phase of research to solve the high-transition region experimental difficulties mentioned above and to investigate the fracture modes in the miniature specimens. For the MNT to be valid, fracture behavior similar to that obtained in the conventional specimens at 41 J must be demonstrated. The punch and anvil dimensions were decreased to allow more bending at the higher temperatures. The design modifications proved successful and high-temperature miniature specimen data were obtained.

An interesting aspect of the fracture appearance is the shape of the crack front. The conventional Charpy specimens exhibit a convex crack front when viewed with the notch closest to the observer. This indicates that the stress intensity is highest near the center of the specimen, and the crack therefore initiates near the center of the notch. The miniature specimens show a

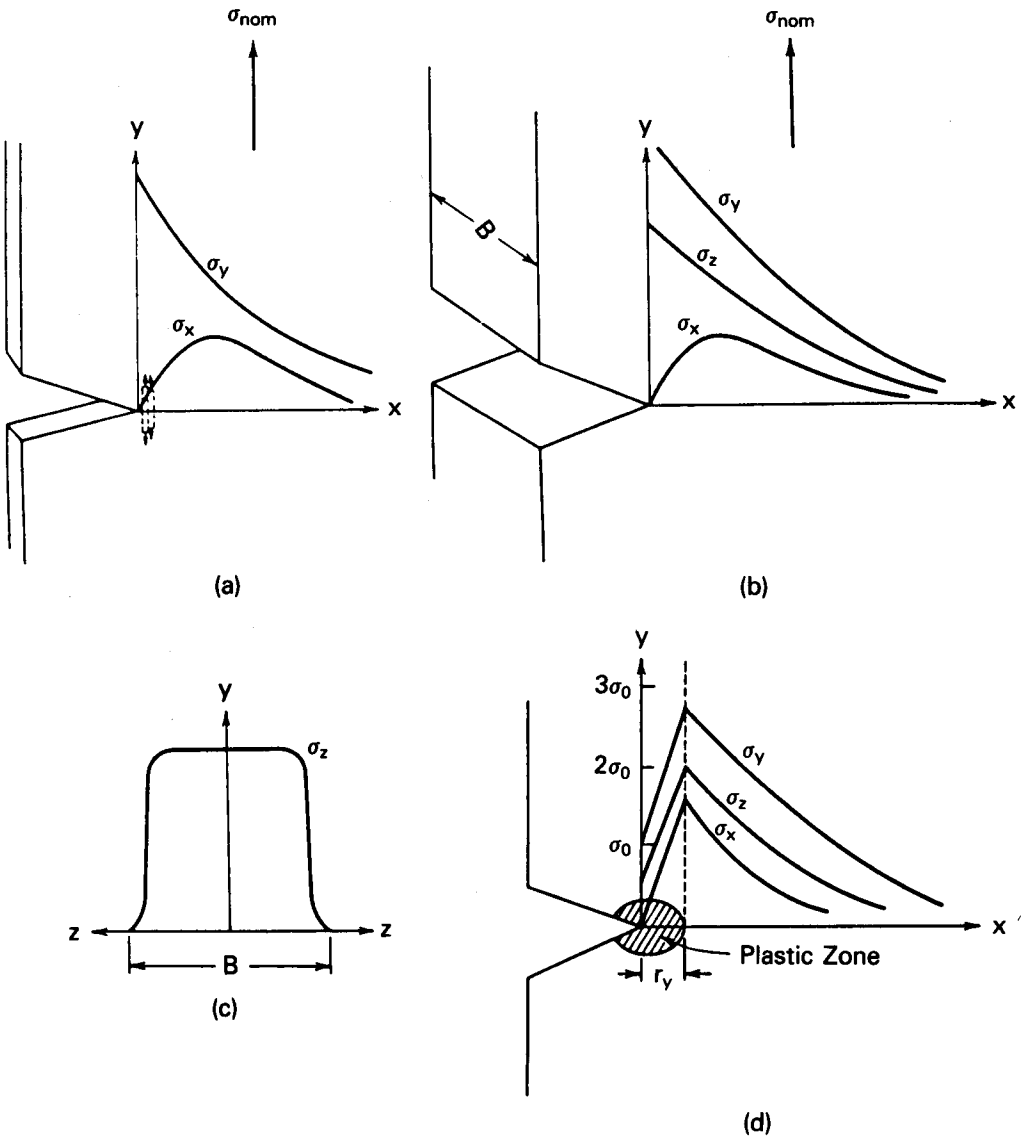

Fig. 3. Schematic of crack tip stress fields.[24]

concave crack front, suggesting that crack initiation occurs near the side grooves. The presence of the side grooves in the miniature specimens results in an increase in the stress level near the side grooves, and the stresses are high enough to initiate the crack in this region of the specimen. Birbeck and Wraith[28] have shown that these crack front shapes indicate that the appearance of the full-width crack at the notch root does not necessarily coincide with maximum load. As discussed later, we have assumed this to be the case in all the calculations reported herein. In future work, crack initiation could be investigated experimentally using electric-potential techniques.

Fracture appearance measurements were made from photographs of the broken surfaces of the specimens using a planimeter. Fracture appearance is not used in the nuclear industry as a measure of the ductile-brittle transition due to the subjective nature of the usual methods of measurement and because considerable effort is needed to obtain accurate data. Additionally, the regulations defining the transition temperature call for the energy-based 41-J index alone and not for the measurement of fracture appearance.[29] We believe, however, that the measurement technique used in this study permits using fracture appearance as an accurate quantitative measure of the brittle-ductile transition for both the miniature and conventional specimens.

The normalized energy data and the fracture appearance data were correlated using the MCFRAC code (Figs. 6 and 7). As can be seen, it is possible to plot a single curve for the standard or the miniature

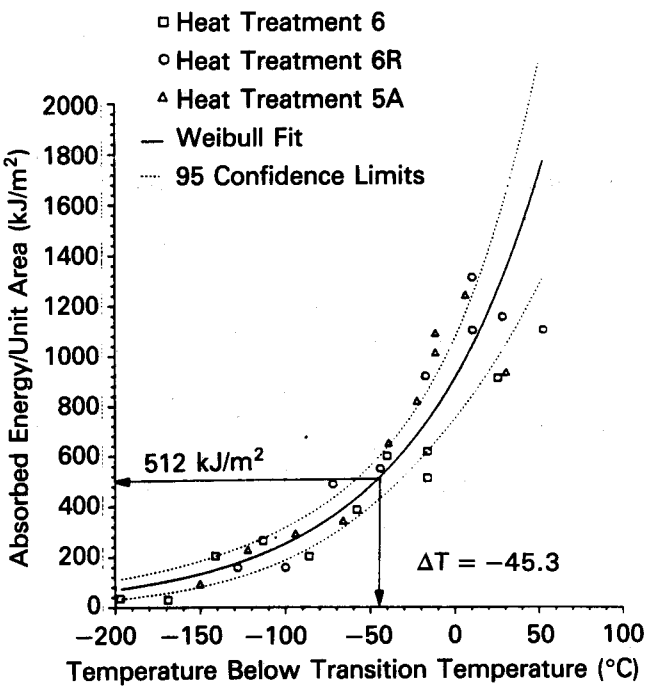

Fig. 4. Energy absorbed in slow-bend fracture of standard Charpy specimens within the ductile-brittle transition region.

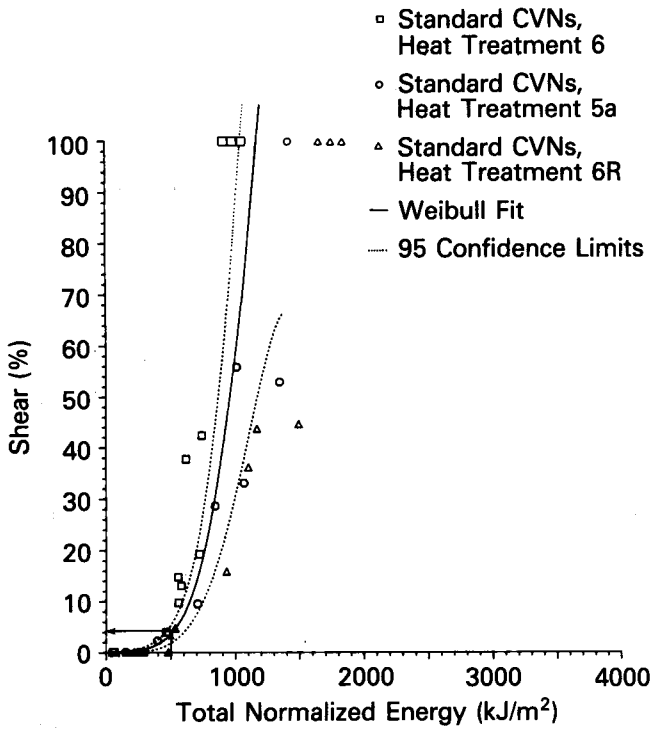

Fig. 6. Normalized total energy as a fracture transition criterion (standard CVNs).

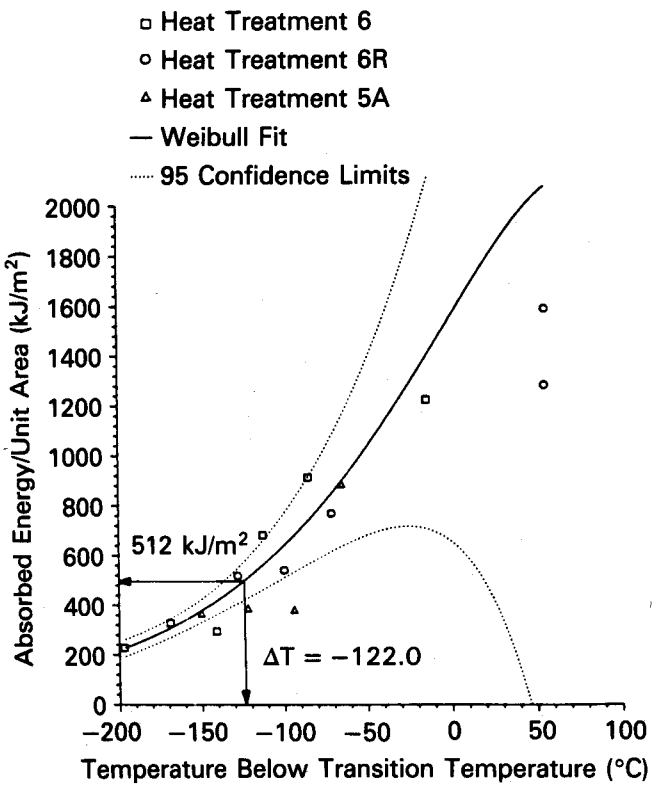

Fig. 5. Energy absorbed in slow-bend fracture of miniaturized specimens within the ductile-brittle transition region.

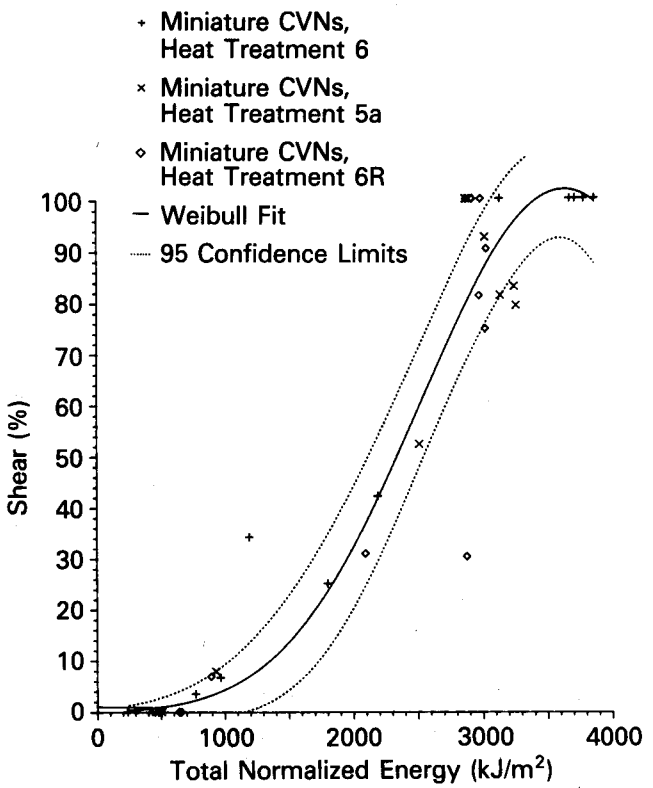

Fig. 7. Normalized total energy as a fracture transition criterion (miniature CVNs).

specimens for all three materials. However, it is obvious that the curves for the two specimen types are not coincident for both the energy and normalized energy parameters. When the 512 kJ/m^2 index is used to compare the fracture appearance for both sizes of specimens based on the normalized energy parameter, it is apparent that 512 kJ/m^2 corresponds to ~4% shear fracture area for the standard specimens, but to ~1% shear for the miniature specimens.

If total absorbed energy is compared in this way to fracture appearance, the disparity between the miniature and standard specimens is even greater, as expected, given the large differences in the specimen sizes (see Figs. 8 and 9). The miniature specimens at 41 J correspond to >70% shear, compared to ~4% for the standard specimens. It can be seen from a comparison of Figs. 8 and 9 that the miniature specimens require less total energy to achieve a given value of percent shear than the conventional CVNs. However, when the normalized energy is used, it is apparent that the miniature specimens seem to require more energy per unit fracture surface area to achieve a given level of percent shear than do the conventional CVNs. This observation suggests that the reasonable results obtained using the energy normalization parameter are fortuitous and may not hold for other materials. These results are summarized in Table III.

These observations indicate that using normalized energy as a parameter and 512 kJ/m^2 as an index for miniature specimens may not be generally applicable. The reasonable data obtained thus far may be attributed to the fortuitously small difference in fracture appearance between standard and miniature specimens at the 512 kJ/m^2 level.

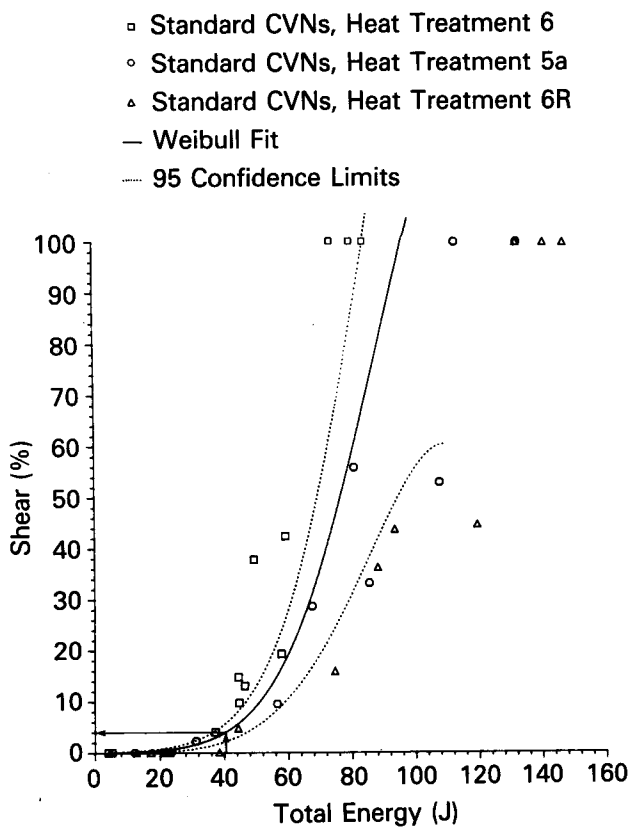

Fig. 8. Nonnormalized total energy as a fracture transition criterion (standard CVNs).

Percent Postmaximum Load Energy

The analyses in the previous section lead to the conclusion that total absorbed energy, whether normalized or not, is probably not a generally applicable MNT parameter. While it has been established that

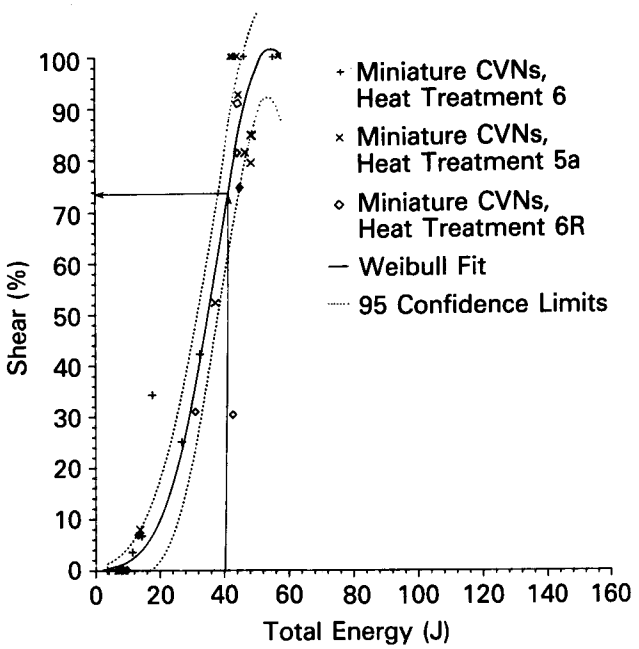

Fig. 9. Nonnormalized total energy as a fracture transition criterion (miniature CVNs).

TABLE III

Percent Shear Fracture Appearance for MNT and Conventional Charpy Specimens for Two Indices

	Percent Shear Fracture Area at 512 kJ/m^2	Percent Shear Fracture Area at 41 J
Standard specimens[a]	~4	~4
Miniature specimens[a]	~1	>70

[a]All three materials.

fracture appearance can serve as a useful parameter for any specimen size, accurate measurement is tedious. In addition, in the nuclear industry, current regulations require the 41-J index transition temperature. Therefore, it is desirable to develop a parameter and index that can be easily related to this energy criterion. Further, a parameter obtained from the load-deflection traces would be more amenable to automated or computerized data acquisition techniques.

It is well established[30] that the total energy absorbed in fracturing a specimen can be partitioned into pre- and postmaximum load energies. The premaximum load energy can be partitioned into elastic stored energy, crack formation energy, and plastic deformation energy. The miniature specimen differs from the conventional one in size and in geometry. Since the miniature specimen has a different span-to-width ratio, different anvil and punch geometry, and has side grooves, the crack initiation energy and its ratio to total energy is different in the two specimen types and therefore is not a useful parameter.

The postmaximum load energy (PME) can be partitioned into elastic stored energy, plastic deformation energy, and stable crack propagation energy. The elastic stored energy is available to drive the cleavage fracture for tests conducted in the transition region. The remaining PME is associated with the plastic deformation work and work that goes into propagating a stable crack. We therefore reasoned that the PME would be less sensitive to differences in specimen geometry and would correlate well with fracture appearance, i.e., percent shear. We assumed in the analysis that the onset of the maximum load corresponds to crack initiation. While this assumption is reasonable for some materials and test temperatures, it was not actually measured in the test program. In future studies, this question should be resolved by using electric potential during testing.

By partitioning the total energy into pre- and postmaximum load energies and plotting these against testing temperature, it can be shown, as expected, that the premaximum load energy does not show a conspicuous transition in fracture behavior. As stated earlier, premaximum load energy is associated with elastic stored energy, crack initiation, and plastic deformation near the notch. On the other hand, the PME exhibits a distinct transition, because this parameter is directly associated with the fracture process. Figures 10 and 11 illustrate this behavior for the heat treatment 6 material. The other two materials, 5A and 6R, exhibit the same behavior.

We defined crack initiation as the complete formation of a full-width crack across the length of the notch. Our theory is that if crack initiation, as defined here, is complete when maximum load is reached, the PME should correlate with percent shear for various specimen sizes and shapes regardless of material. Assuming this to be the case, it was thus considered theoretically sound to use PME as a parameter for ductile fracture transition characterization. Differences in specimen size result in the absolute values of PME being different among specimen types. However, the relative proportion of the energy that goes into crack propagation and plastic deformation should correlate with fracture appearance for specimens of different sizes and shapes. We decided, therefore, to convert the absolute values of PME to percentages by dividing by the total energy (excluding shear lip formation energy). As stated previously, the total energy used in the calculations is defined as the sum of the absorbed energy up to the onset of cleavage. Therefore, any energy

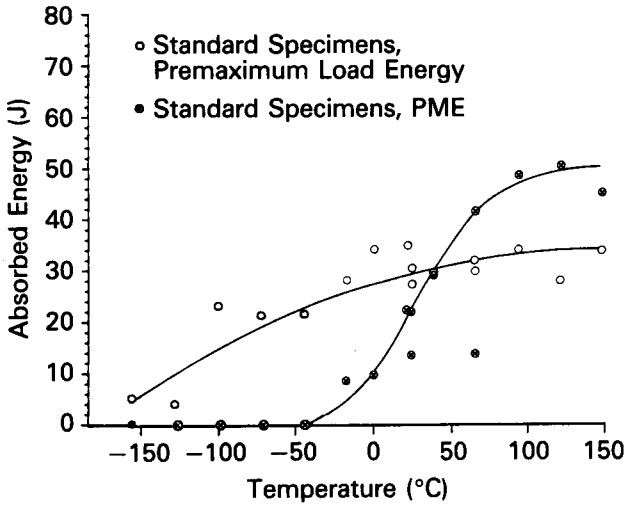

Fig. 10. Pre- and postmaximum load energies compared (standard specimens, heat treatment 6).

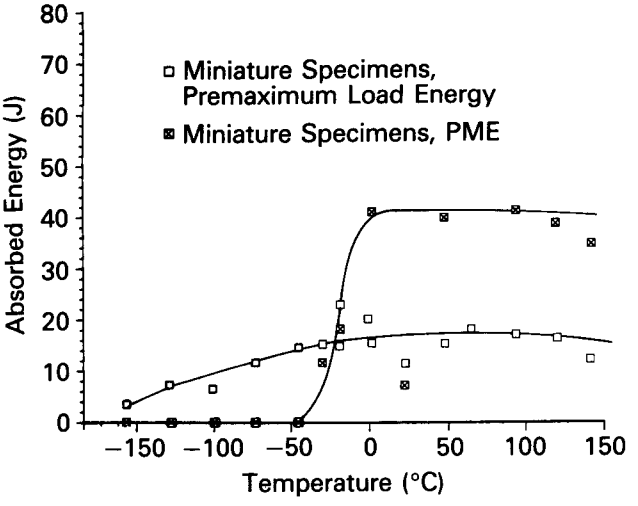

Fig. 11. Pre- and postmaximum load energies compared (miniature specimens, heat treatment 6).

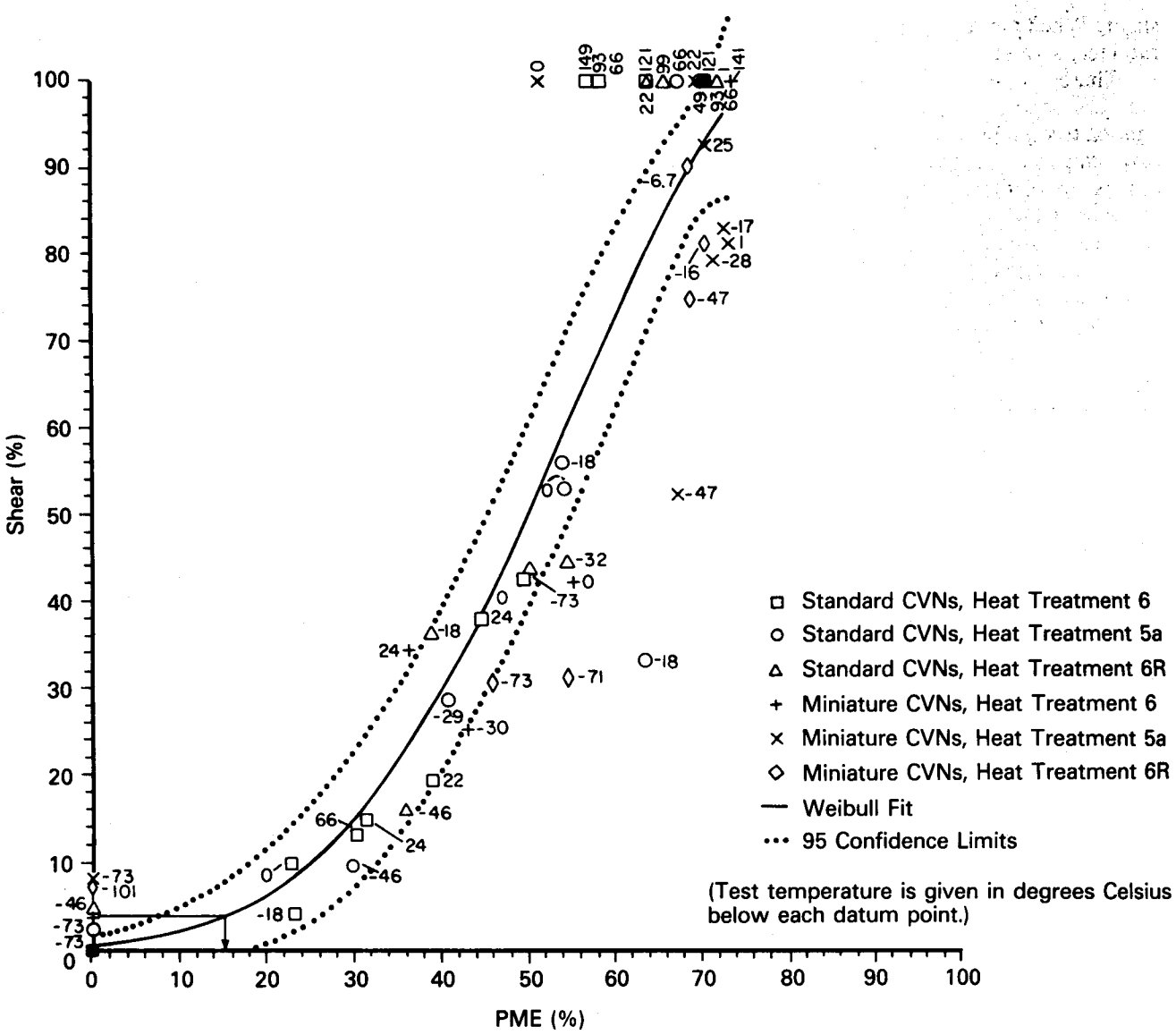

Fig. 12. Percent PME as a fracture transition criterion (both specimen sizes).

absorbed in the formation of shear lips was not included. A MCFRAC plot of percent shear fracture appearance versus percent PME is given in Fig. 12. This figure shows that the data for all three materials in both specimen geometries fit the same curve. A correlation of this kind now allows the use of two criteria, one based on energy and the other on fracture appearance. It is recognized that this correlation is most likely material dependent.

Figure 12 is central to the validation of the MNT. Future work should attempt further benchmarking for other materials. We believe that the scatter in the upper end of the transition region may be due to uncertainty in the crack initiation energy determination described earlier.

TRANSITION TEMPERATURE INDICES

The data analysis techniques described earlier allow the use of percent shear fracture appearance and percent PME as MNT parameters, with new indices to be defined based on the 41 J or any other index of interest. Figure 12 provides the correlation for obtaining these indices for both specimen dimensions. This technique can be used to relate any specimen geometries that yield fracture transition data. Thus, from Figs. 6 and 8 for the standard CVNs, a Charpy energy level of 41 J corresponds to ~4% shear fracture appearance. Referring to Fig. 12, this level of shear corresponds to ~15% PME. Thus, when fracture appearance is used as the MNT parameter, the corresponding index is 4%

shear. When percent PME is chosen as the MNT parameter, a value of 15% PME is used as the index.

Therefore, when the parameters of percent shear fracture appearance or percent PME are plotted against test temperature (Figs. 13 through 18), transition temperatures for each material may be obtained at these new index levels (4% shear and 15% PME, respectively). Since these data are plotted separately for each material and specimen type and hence are rather sparse, the curves were fit using SAS/GRAPH statistical procedures. Future work should be directed toward obtaining more data in the range of the Charpy indices. At present, it appears that the MNT specimens yield accurate data. However, this finding must be confirmed in the future for other materials and more data gathered at the 15% PME level. Table IV summarizes these transition temperatures.

On comparing these transition temperatures with the standard dynamic CVN transition temperatures, correction factors due to rate effect and size effect are obtained. This is illustrated schematically in Fig. 19. The average shift due to rate effect for the conventional CVN is 45.3°C (Ref. 31). This shift was determined by averaging the static to dynamic shift at the 41-J level for the three materials using conventional Charpy specimens. As discussed earlier, this is

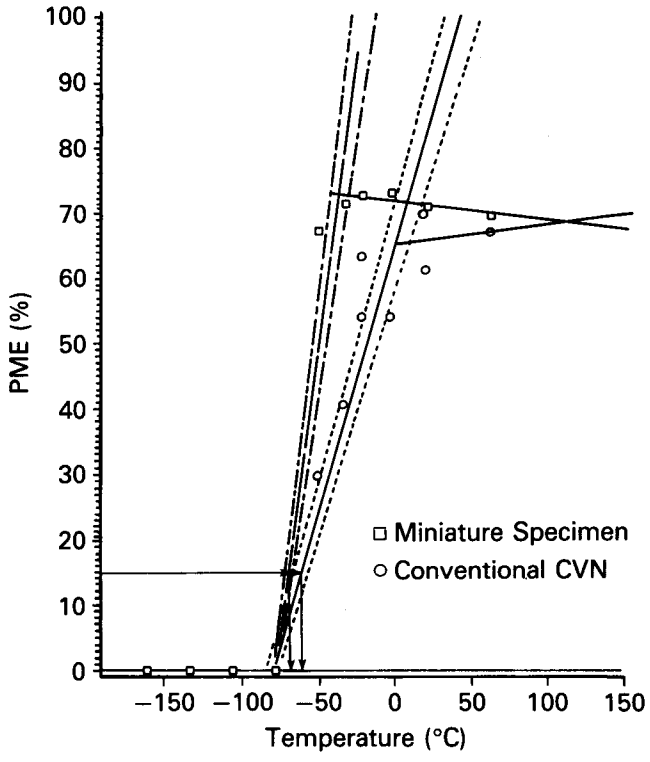

Fig. 14. Transition temperature from 15% PME index (heat treatment 5A material, both specimen sizes).

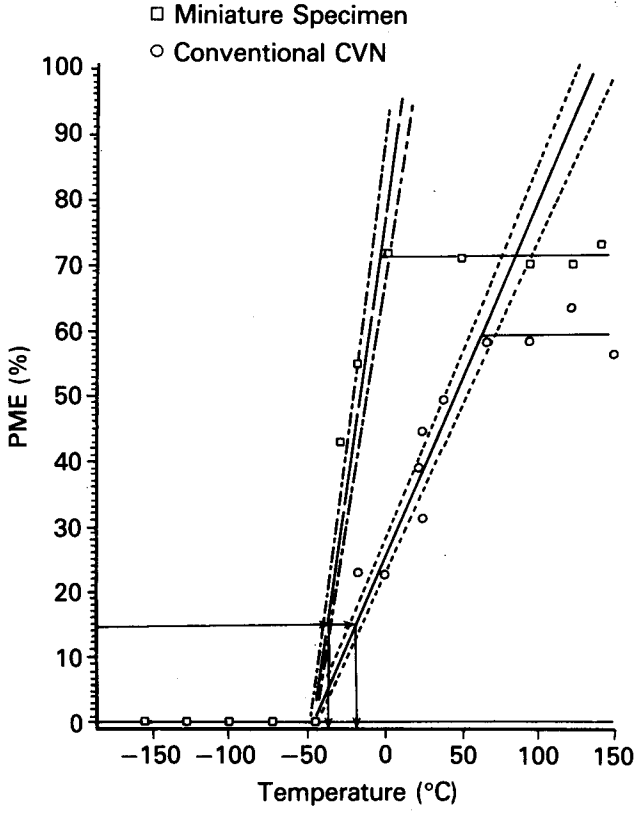

Fig. 13. Transition temperature from 15% PME index (heat treatment 6 material, both specimen sizes).

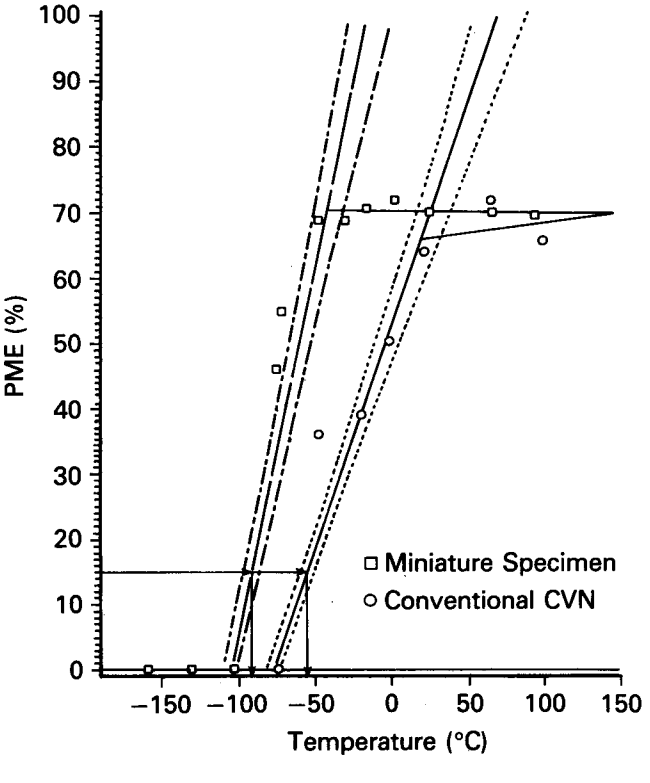

Fig. 15. Transition temperature from 15% PME index (heat treatment 6R material, both specimen sizes).

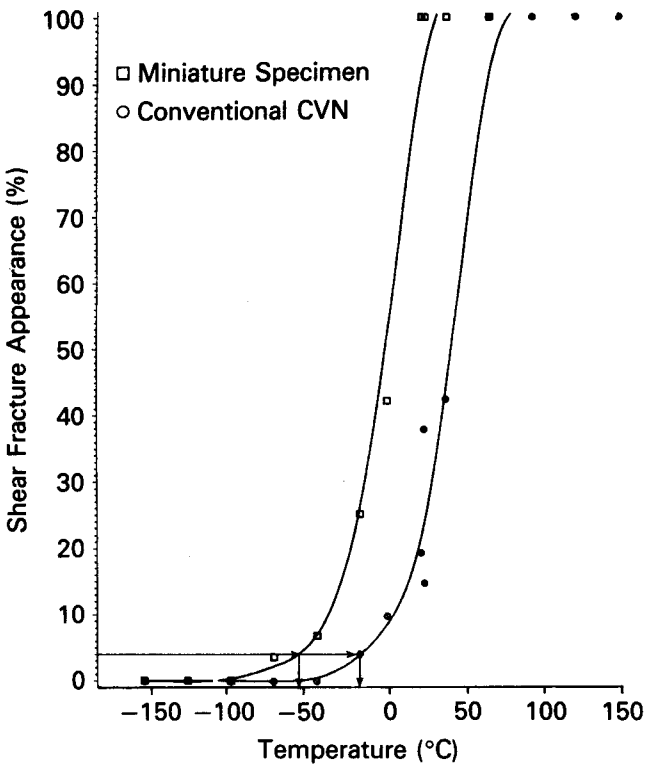

Fig. 16. Transition temperature from 4% shear fracture appearance index (heat treatment 6 material, both specimen sizes).

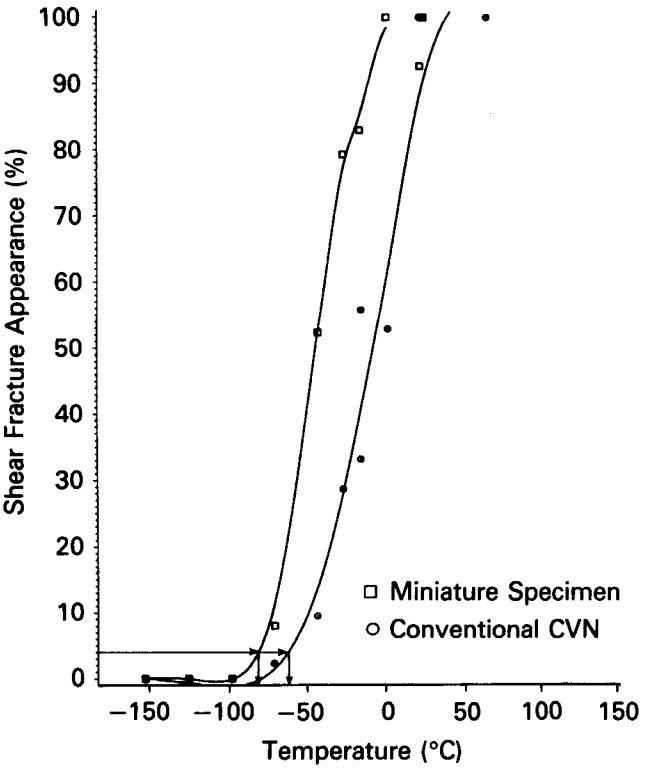

Fig. 17. Transition temperature from 4% shear fracture appearance index (heat treatment 5A material, both specimen sizes).

in reasonable agreement with the correlation presented in Ref. 27.

Table V presents the shifts due to rate and size effects using the 4% shear and 15% PME indices. The data in Table V can be used to relate the MNT data with conventional, dynamic Charpy data for the ASTM A508 steel. For example, suppose this material were irradiated and the 4% shear index is used to analyze the MNT data. If the MNT data for the irradiated material yielded a 4% shear transition temperature of 50°C, then the dynamic 41-J transition temperature is obtained by adding the rate effect shift (53.3°C) and the size effect shift (30.7°C) to yield a 41-J dynamic conventional Charpy transition temperature of 134°C. This is the approach that would be used in cases where the MNT was run on irradiated pressure vessel steels, and there is no archival material available for testing.

In cases where unirradiated archival material is available, it is possible to machine unirradiated and irradiated MNT specimens and measure the shift directly. The strategy would be to first develop the unirradiated MNT data, test the surveillance capsule

TABLE IV

Standard CVN and MNT Slow-Bend Transition Temperatures

Indices	Heat Treatment					
	6		5A		6R	
	Standard CVN [°C (°F)]	MNT [°C (°F)]	Standard CVN [°C (°F)]	MNT [°C (°F)]	Standard CVN [°C (°F)]	MNT [°C (°F)]
15% PME	−18 (0)	−37 (−35)	−57 (−70)	−65 (−85)	−54 (−65)	−90 (−130)
4% Shear	−18 (0)	−57 (−70)	−62 (−80)	−84 (−120)	−76 (−105)	−107 (−160)

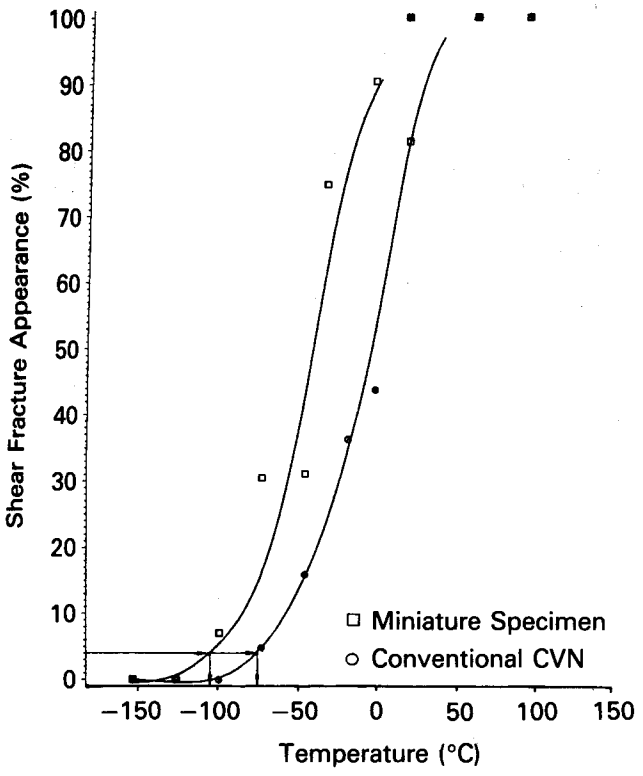

Fig. 18. Transition temperature from 4% shear fracture appearance index (heat treatment 6R material, both specimen sizes).

Charpy specimens, machine the irradiated MNT specimens from the broken Charpy specimens, and test and/or reinsert the MNT specimens back in the reactor to generate plant life extension data.

A comparison of the transition temperature shift data for the ASTM A508 steel is summarized in Table VI. This material was temper embrittled to simulate neutron irradiation effects. The MNT transition temperature shifts compare well with the conventional dynamic Charpy data. The MNT data are sparse for some of the materials, and the accuracy of the MNT data is expected to improve with more research. Overall, the MNT data fall within the experimental uncertainty for transition temperature testing. It is interesting to note that the MNT shifts are consistently ~20°C lower than the 41-J dynamic shift. Further study is needed to determine if a shift correction is needed. Comparison of the difference in the shift for the conventional dynamic Charpy and MNT specimens shown in Table VI indicates the robust nature of the MNT parameters and indices.

SUMMARY AND CONCLUSIONS

The miniaturized specimen design required only 6% of the volume of a standard Charpy specimen. These specimens have proven satisfactory for measuring transition temperature shifts due to heat treatment

TABLE V

Shifts Due to Rate and Size Effects

	Standard Specimen Impact Transition Temperature (°C)	Standard Specimen Slow-Bend Transition Temperature (°C)	MNT Specimen Slow-Bend Transition Temperature (°C)	(Rate Effect) Standard Specimen Impact to Slow-Bend Shift (°C)	(Size Effect) Standard Slow-Bend to MNT Slow-Bend Shift (°C)
Heat Treatment	41 J	4% Shear Index			
6	40	−18	−57	58	39
5A	−7	−62	−84	55	22
6R	−29	−76	−107	47	31
Average rate effect shift: 53.3°C Average size effect shift: 30.7°C					
Heat Treatment	41 J	15% Normalized PME Index			
6	40	−18	−37	58	19
5A	−7	−57	−65	50	8
6R	−29	−54	−90	25	36
Average rate effect shift: 44.1°C Average size effect shift: 21.3°C					

TABLE VI

Simulated Neutron Irradiation Transition Temperature Shift Data*

Material Condition	Standard Specimen 41-J Dynamic Transition Temperature Shift (°C)	Standard Specimen Slow-Bend Transition Temperature Shift Based on 4% Shear (°C)	Miniature Specimen Slow-Bend Transition Temperature Shift Based on 4% Shear (°C)	Standard Specimen Slow-Bend Transition Temperature Shift Based on 15% Normalized PME (°C)	Miniature Specimen Slow-Bend Transition Temperature Shift Based on 15% Normalized PME (°C)
Irradiation simulation 1 (6 to 5A)	47	44	27	39	28
Irradiation simulation 2 (6 to 6R)	69	58	50	36	53
Difference in shifts	22	14	23	−3	25

*The shift due to neutron irradiation was simulated by heat treatment.

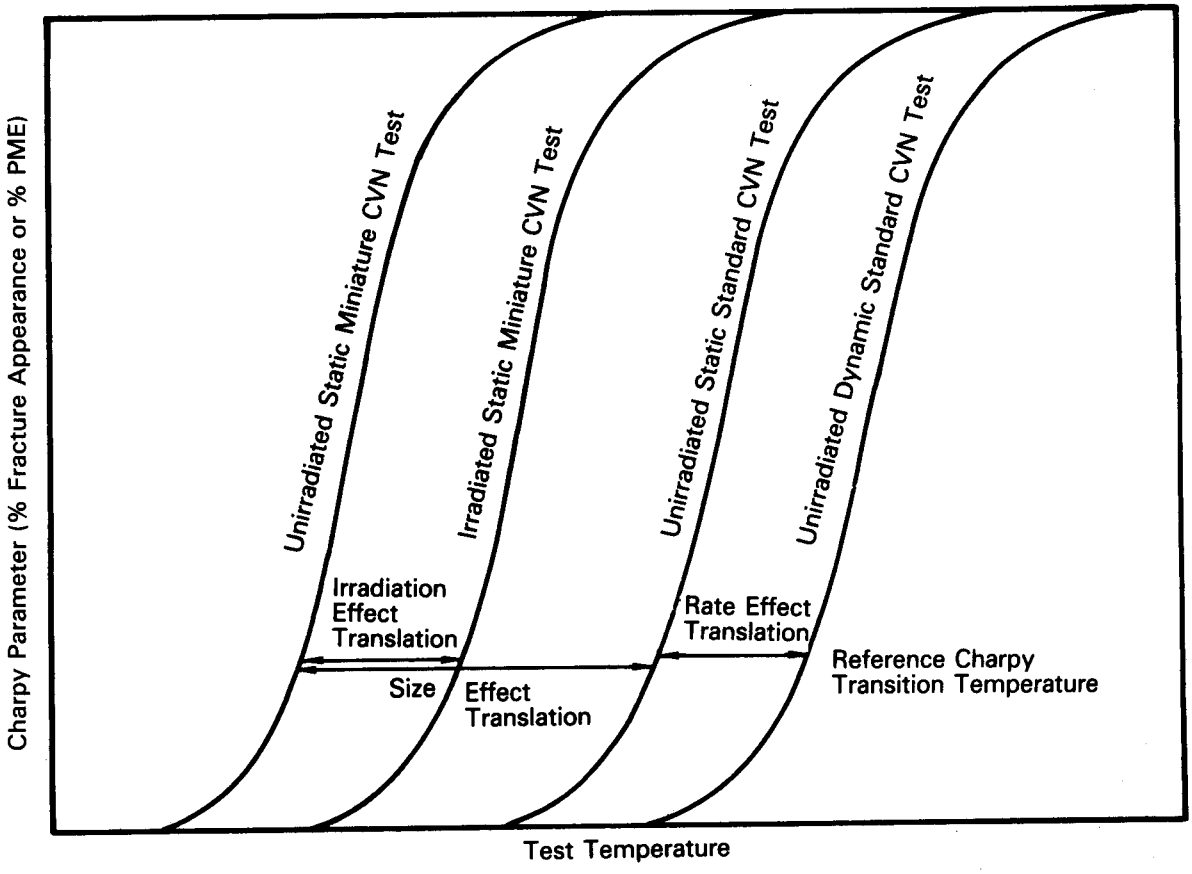

Fig. 19. Relationship between reference Charpy transition temperature and irradiated miniature Charpy slow-bend transition temperature.

of a reactor-grade pressure vessel steel. Fracture appearance has been demonstrated to be a useful miniature specimen parameter. For applications in the nuclear industry, conventional dynamic ASTM A508 steel Charpy specimens exhibit ~4% shear at the 41-J energy level. Therefore, the appropriate index for miniature specimens is 4% shear for this material. The 512 kJ/m^2 index was found to be useful with the

ASTM A508 steel studied; however, future use of this index requires a fracture mode investigation.

A new parameter, percent normalized PME, which is easier to use than fracture appearance, has been benchmarked for an ASTM A508 steel. This parameter is easier to use than fracture appearance, since the data analysis can be easily automated. Like fracture appearance, percent normalized PME can be used to relate miniature specimen data with conventional dynamic, ASTM E23 specimen data. For the ASTM A508 material investigation, the result is a 41-J DBTT with accuracy equal to that obtained using conventional ASTM test practices. The data obtained thus far are sparse at the 15% normalized PME level. Future studies should provide data at the 15% normalized PME level to more accurately assess the uncertainty of the method.

ACKNOWLEDGMENTS

We would like to express our thanks to Battelle's Office of Corporate Technical Development for funding part of this work. The invention was made prior to employment at Battelle; however, most of the work was performed while Dr. Manahan was employed at Battelle and Mr. Charles was a graduate student at The Ohio State University.

REFERENCES

1. M. P. MANAHAN, A. S. ARGON, and O. K. HARLING, "The Development of a Miniaturized Disk Bend Test for the Determination of Postirradiation Mechanical Properties," *J. Nucl. Mater.*, **103 & 104**, 1545 (1981).

2. M. P. MANAHAN, R. KOHLI, J. SANTUCCI, and P. SIPUSH, "A Phenomenological Investigation of In-Reactor Cracking of Type 304 Stainless Steel Control Rod Cladding," *J. Nucl. Eng. Design*, **113**, 297 (1989).

3. M. P. MANAHAN et al., "Fracture Toughness of Irradiated ASTM A212B Pressure Vessel Steel," Battelle Memorial Institute (Sep. 1988).

4. M. P. MANAHAN, "Determining the Physical Properties of Steam Generator Tube Scale Using Miniature Specimens," *J. Nucl. Technol.* (in press).

5. M. P. MANAHAN, "Surveillance Capsules A′ and C′ for Nine Mile Point Unit 1," Battelle Memorial Institute (Sep. 1987).

6. C. CHARLES, "A Generalized Methodology for Rationalizing Charpy Data from Test Specimens of Widely Divergent Dimensions," MS Thesis, The Ohio State University (1987).

7. "Mechanical Testing of Steel Products," ASTM Standard A370-86a, American Society for Testing Materials (1986).

8. "Notched Bar Impact Testing of Metallic Materials," ASTM Standard E23-86, American Society for Testing Materials (1986).

9. "Plane-Strain Fracture Toughness of Metallic Materials," ASTM Standard E399-83, American Society for Testing Materials (1983).

10. "Test Method for J_{Ic}, A Measure of Fracture Toughness," ASTM Standard E813, American Society for Testing Materials (1974).

11. "Drop-Weight Tear Tests of Ferritic Steels," ASTM Standard E436-74, American Society for Testing Materials (1974).

12. "Sharp-Notch Tension Testing of High-Strength Sheet Materials," ASTM Standard 338-78, American Society for Testing Materials (1974).

13. "Sharp-Notch Tension Testing with Cylindrical Specimens," ASTM Standard E602-81, American Society for Testing Materials (1981)

14. "Dynamic Tear Testing of Metallic Materials," ASTM Standard E604-83, American Society for Testing Materials (1983)

15. "Fracture Testing with Surface-Crack Tension Specimens," ASTM Standard E740-80, American Society for Testing Materials (1980).

16. "R-Curve Determination," ASTM Standard E561-86, American Society for Testing Materials (1986).

17. "Fracture Testing," ASTM Standard E616-80, American Society for Testing Materials (1980).

18. "Conducting Drop-Weight Test to Determine Nil-Ductility Transition Temperature of Ferritic Steels," ASTM Standard E208-85, American Society for Testing Materials (1985).

19. W. R. CORWIN and A. M. HOUGHLAND, "Effect of Specimen Size and Material Condition on the Charpy Impact Properties of 9 Cr-1 Mo-V-Nb Steel," *The Use of Small-Scale Specimens for Testing Irradiated Material*, ASTM-STP 888, p. 337, W. R. CORWIN and G. E. LUCAS, Eds., American Society for Testing Materials (1986).

20. G. E. LUCAS, G. R. ODETTE, J. W. SHECKHERD, P. McCONNELL, and J. PERRIN, "Subsized Bend and Charpy V-Notch Specimens for Irradiated Testing," *The Use of Small-Scale Specimens for Testing Irradiated Material*, ASTM-STP 888, p. 322, W. R. CORWIN and G. E. LUCAS, Eds., American Society for Testing Materials (1986).

21. P. McCONNELL, J. W. SHECKHERD, J. S. PERRIN, and R. A. WULLAERT, *The Use of Small-Scale*

Specimens for Testing Irradiated Material, ASTM-STP 888, p. 367, W. R. CORWIN and G. E. LUCAS, Eds., American Society for Testing Materials (1986).

22. M. P. MANAHAN, "Determination of Fracture Behavior of Ferritic Steels Using Miniaturized Specimens," *J. Nucl. Mater.*, **166**, 321 (1989).

23. R. D. CHEVERTON et al., "Pressure Vessel Fracture Studies Pertaining to the PWR Thermal-Shock Issue: Experiments TSE-5, TSE-5A, and TSE-6," ORNL-6163, Oak Ridge National Laboratory (1985).

24. G. E. DIETER, *Mechanical Metallurgy*, 2nd ed., Chap. 7, McGraw-Hill, New York (1976).

25. M. P. MANAHAN, A. R. ROSENFIELD, and S. F. QUAYLE, "Statistical Methodology for Analysis of Fracture Mechanics Data," Battelle Columbus Laboratories (Jan. 1985).

26. M. P. MANAHAN, S. QUAYLE, A. R. ROSENFIELD, and D. K. SHETTY, "Statistical Analysis of Cleavage-Fracture Data," presented at Int. Conf. Fatigue, Corrosion Cracking, Fracture Mechanics, and Failure Analysis, Salt Lake City, Utah, December 2–6, 1985 (1985).

27. S. T. ROLFE and J. M. BARSOM, *Fracture and Fatigue Control in Structures*, Prentice-Hall, Englewood Cliffs, New Jersey (1977).

28. G. BIRBECK and A. E. WRAITH, "Influence of Crack Shape or Crack Opening Displacement Measurements Using Charpy Specimens," *Metallurgical Trans.*, **1**, 1474 (May 1970).

29. "Leakage Rate Testing of Containments of Light-Water-Cooled Nuclear Power Plants," *Code of Federal Regulations*, Title 10, Part 50 (1979).

30. R. W. HERTZBERG, *Deformation and Fracture Mechanics of Engineering Materials*, John Wiley & Sons, New York (1983).

31. M. P. MANAHAN, A. R. ROSENFIELD, and J. A. VANECHO, "Final Report on Miniaturized Fracture Mechanics Feasibility Study to Corporate Technical Development," Battelle Columbus Laboratories (1985).